JOURNAL OF GUIDANCE, CONTROL, AND DYNAMICS
Vol. 17, No. 4, July–August 1994

Guidance Law for Hypersonic Descent to a Point

G. Richard Eisler*
Sandia National Laboratories, Albuquerque, New Mexico 87185
and
David G. Hull†
University of Texas at Austin, Austin, Texas 78712

A neighboring optimal control problem is formulated for a hypersonic glider to execute a maximum-terminal-velocity descent to a stationary target. The resulting two-part, feedback control scheme initially solves a nonlinear algebraic problem to generate a nominal trajectory to the target altitude. Second, a neighboring optimal path computation about the nominal provides the lift and side-force perturbations necessary to achieve the target downrange and crossrange. On-line feedback simulations of the proposed scheme and a form of proportional navigation are compared with an off-line parameter optimization method. The neighboring optimal terminal velocity compares very well with the parameter optimization solution and is far superior to proportional navigation. A variety of targeting geometries are possible, demonstrating flexibility in use.

Introduction

THE general solution of the optimal flight of a gliding vehicle to arbitrary, but specified, final conditions is a difficult problem that is only partially understood. A variety of approximate analytic solutions exist for subsets of the relevant differential equations and boundary conditions. Few formulations exist to satisfy range or position constraints. In this paper, a midcourse-guidance control law is developed for guiding a hypersonic glider to a fixed point on the ground. The guidance law is based on the lift and side-force coefficient histories that maximize the final velocity. This optimal trajectory has been of continuing interest.

Contensou[1] was the first to consider optimal control and proposed the problem for unconstrained range in terms of flight path angle γ as the independent variable. This work was extended to the general problem of flight in a vertical plane, where control solutions for all manner of constraints could be obtained by integrating a second-order, nonlinear, differential equation.[2] However, numerical results were presented only for constrained final γ and altitude. No *closed-form* control solution exists for maximizing velocity at a fixed point. In this paper, the authors extend the work done on maximizing terminal velocity for a constrained downrange and altitude[3] to include a constrained crossrange. In the previous effort, it was assumed the glider is cruising at constant altitude and knows the position of the fixed target in the vertical plane. At each sample point, the commanded control was the sum of the optimal unconstrained range control, which would take the vehicle near the target, and the neighboring optimal control,[4,5,6] which would enable the vehicle to hit the target. Crossrange errors, which might arise from wind gusts, nonaveraged vehicle asymmetry effects, or initial conditions, are now considered. Throughout this study, it is assumed that Loh's approximation[7] is valid, but it is updated, as are the states, at every sample point.

Development of the guidance rule will proceed similarly to that in Ref. 3. First, the lift coefficient history, which maximizes the final speed at a fixed, final altitude, but unconstrained, final downrange and crossrange, is determined analytically. The fixed-final downrange and crossrange constraint equations are included to facilitate the derivation of the neighboring optimal control. Second, the perturbation in the lift and side-force coefficient histories, which enable the glider to meet the surface position constraints, are derived. No constraints of a thermal or load-factor nature were considered. Although the target has been assumed to be fixed, this formulation is sufficiently general to apply to a moving target, if the target location is assumed known from an on- or off-board source.

To verify the midcourse guidance rule, it is flown in a three-DOF simulation of a hypersonic glider and is shown to guide the vehicle to the target. Also, the guided trajectory is shown to compare favorably with the maximum final velocity trajectory of the simulation (found by a parameter optimization method). Finally, results are presented to establish the robustness of the guidance law to various target locations and to establish the superiority of the guidance law to that of proportional navigation.

Optimal Control

A schematic of the guidance rule is shown in Fig. 1. At a sample point, the maximum final velocity trajectory to the ground (unconstrained surface range) is calculated and is assumed to pass near the target. This could be accomplished by a vehicle loitering at altitude, continuously computing unconstrained-range trajectories, and initiating descent only when the unconstrained-range end point is "close" to the target. Next, the neighboring optimal path to the target (perturbed final point) is obtained. The perturbation in the lift coefficient is added to the optimal lift coefficient to form the desired lift control. The perturbation in the side-force coefficient *is* the desired side-force value (because its optimal value is zero). These controls are held constant over a sample period, and the process is repeated at the next sample point. Note that in the case of crossrange perturbations, the nominal optimal solution is also vertical planar flight.[3] This plane is continually orienting itself to the true target heading as updates are made at each sample point. The fixed surface position constraints are included in the derivation of the unconstrained surface range optimal trajectory to facilitate the derivation of the neighboring optimal trajectory.

The equations of motion for a nonthrusting, point mass traveling in a plane over a spherical, nonrotating Earth at an altitude that is small with respect to the radius of the Earth are

Received Feb. 11, 1993; revision received Oct. 6, 1993; accepted for publication Oct. 28, 1993.

*Member of the Technical Staff, Structural Dynamics Division. Associate Fellow AIAA.

† M. J. Thompson Regents Professor, Department of Aerospace Engineering. Associate Fellow AIAA.

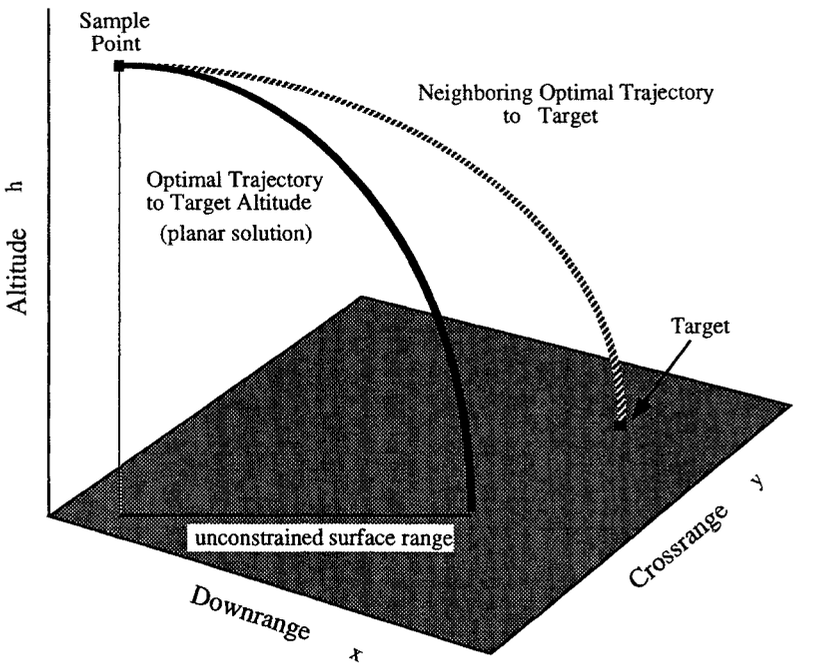

Fig. 1 Guidance schematic.

$$\dot{x} = V\cos\gamma\cos\chi$$
$$\dot{y} = V\cos\gamma\sin\chi$$
$$\dot{h} = V\sin\gamma$$
$$\dot{V} = \frac{-\tfrac{1}{2}\rho V^2 S_R C_D}{m} - g_s\sin\gamma \tag{1}$$
$$\dot{\gamma} = \frac{\tfrac{1}{2}\rho V^2 S_R C_L}{mV} - \left(\frac{g_s}{V} - \frac{V}{r_s}\right)\cos\gamma$$
$$\dot{\chi} = \frac{\tfrac{1}{2}\rho V^2 S_R C_S}{mV\cos\gamma}$$

where $(\cdot) = \mathrm{d}(\,)/\mathrm{d}t$, x is downrange, y is crossrange, h is altitude, V is velocity, γ is flight path angle, χ is heading angle, ρ is atmospheric density, g_s is the gravitational constant at the Earth's surface, r_s is the Earth radius, S_R is the vehicle reference area, m is the vehicle mass, and C_L, C_S, C_D are the lift, side-force, and drag coefficients, respectively.

In the derivation of the optimal trajectory, the following additional assumptions are made: 1) flight in a great circle plane over a spherical Earth with an exponential atmosphere of scale height β, 2) gravitational force is small with respect to the aerodynamic force in the $\dot{V}$ equation, 3) parabolic drag polar $C_D = C_{D_o} + KC_L^2 + KC_S^2$ with constant coefficients where $\sqrt{C_{D_o}/K} = C_L^*$ is the lift coefficient for maximum lift-to-drag ratio, and 4) Loh's approximation is valid [$\overline{M} \approx$ constant in Eq. (7)]. The equations of motion can be written in terms of nondimensional variables as

$$\frac{\mathrm{d}\xi}{\mathrm{d}\phi} = -\frac{\cos\phi\cos\chi}{w(\lambda + \overline{M})} \tag{2}$$
$$\frac{\mathrm{d}\eta}{\mathrm{d}\phi} = -\frac{\cos\phi\sin\chi}{w(\lambda + \overline{M})} \tag{3}$$
$$\frac{\mathrm{d}w}{\mathrm{d}\phi} = -\frac{\sin\phi}{(\lambda + \overline{M})} \tag{4}$$
$$\frac{\mathrm{d}u}{\mathrm{d}\phi} = \frac{1 + \lambda^2 + \sigma^2}{(\lambda + \overline{M})} \tag{5}$$
$$\frac{\mathrm{d}\chi}{\mathrm{d}\phi} = -\frac{\sigma}{\cos\phi(\lambda + \overline{M})} \tag{6}$$

where

$$\phi = -\gamma, \qquad \xi = x/\beta, \qquad \eta = y/\beta, \qquad w = \frac{\rho}{2m/(\beta S_R C_L^*)}$$
$$u = \frac{C_L^*}{C_{D_o}}\ln\frac{V}{\sqrt{g_s r_s}}, \qquad \lambda = \frac{C_L}{C_L^*}, \qquad \sigma = \frac{C_S}{C_L^*} \tag{7}$$
$$\overline{M} = \frac{2m\cos\gamma}{C_L^* S_R \rho r_s}\left(1 - \frac{g_s r_s}{V^2}\right)$$

whereas Loh's term, $\overline{M} < 0$, is assumed constant over an optimal trajectory, its value is updated at each sample point.

The optimal control problem is to find the lift and side-force coefficient histories, $\lambda(\phi)$, $\sigma(\phi)$, which maximize the final velocity or *minimize* the performance index $J = -u_f$, subject to state equations, $\mathrm{d}\mathbf{x}/\mathrm{d}\phi = f(\phi, \mathbf{x}, \lambda)$ [Eqs. (2–6)]; initial conditions, ϕ_o, ξ_o, η_o, w_o, u_o, χ_o known; and final conditions,

$$\Psi(\phi_f, x_f) = \begin{bmatrix} \xi_f - \xi_{ur} \\ \eta_f - \eta_{ur} \\ w_f - w_T \end{bmatrix} = 0$$

The quantities ξ_{ur} and η_{ur} are the nondimensional range and crossrange that result along the unconstrained range optimal path. The fixed final position conditions are included here to facilitate the later derivation of the neighboring optimal control. From this problem statement, the Hamiltonian and the Bolza functions are constructed as

$$H = \frac{1}{(\lambda + \overline{M})}\left[-\frac{\cos\phi}{w}(p_\xi\cos\chi + p_\eta\sin\chi)\right.$$
$$\left. - p_w\sin\phi + p_u(1 + \lambda^2 + \sigma^2) - \frac{p_\chi\sigma}{\cos\phi}\right] \tag{8}$$

$$G = -u_f + \nu_1(\xi_f - \xi_{ur}) + \nu_2(\eta_f - \eta_{ur}) + \nu_3(w_f - w_T) \quad (9)$$

where p and ν denote Lagrange multipliers. In what follows it is assumed that the target is located at the position that results if no constraint is imposed on surface range. Hence, $p_\xi = p_\eta = 0$, and $\nu_1 = \nu_2 = 0$ hold.

The differential equations and boundary conditions for p lead to

$$p_\xi = p_\eta = 0, \quad p_w = \nu_3, \quad p_u = -1, \quad p_\chi = 0 \quad (10)$$

meaning that p is constant. Next, the optimality conditions, H_λ, $H_\sigma = 0$ combined with the Legendre condition

$$\begin{bmatrix} H_{\lambda\lambda} & H_{\lambda\sigma} \\ H_{\sigma\lambda} & H_{\sigma\sigma} \end{bmatrix} = \begin{bmatrix} -\dfrac{2}{\lambda + \bar{M}} & 0 \\ 0 & -\dfrac{2}{\lambda + \bar{M}} \end{bmatrix} \geq 0$$

give

$$\lambda + \bar{M} = -\sqrt{1 + \bar{M}^2 + p_w \sin\phi} \quad (11)$$

where part of the solution process has been to show that no inflection point, $d\phi = 0$, can occur along the optimal path.[8] Hence, ϕ is monotonically increasing. (An inflection point would occur at $\lambda + \bar{M} = 0$ where the gravitational and centrifugal forces are balanced by the lift.) The optimality condition $H_\sigma = 0$ produces

$$\sigma = 0 \rightarrow \frac{d\chi}{d\phi} = 0 \rightarrow \chi(\phi) = \chi_o \quad (12)$$

Finally, the natural boundary condition for ϕ_f shows that $\lambda_f = 0$, so that, from Eq. (11)

$$\sin\phi_f = -1/p_w \quad (13)$$

associating the multiplier, $p_w < -1$, directly with a physical quantity.

What remains is to determine the value of p_w from the prescribed boundary conditions. Substitution of Eq. (11) into Eq. (4) and integrating gives

$$w - w_o = \sqrt{2/b}[-F(\Phi, k) + 2E(\Phi, k)]_{\phi_o}^{\phi} \quad (14)$$

where F and E are elliptic integrals of the first and second kinds, and

$$a = 1 + \bar{M}^2 < b = -p_w$$

$$\Phi = \sin^{-1}\left[\frac{b(1 - \sin\phi)}{a + b}\right]^{1/2} \qquad k = \left[\frac{a + b}{2b}\right]^{1/2}$$

Eqs. (13) and (14) applied at the final point can be combined into a single, nonlinear algebraic equation solved by Newton's method for p_w. Once p_w is known, $w(\phi)$ is computed from Eq. (14) and $\lambda(\phi)$ is given by Eq. (11). Finally, $\xi(\phi)$, $\eta(\phi)$, and $u(\phi)$ can be obtained from Eqs. (2), (3), and (5), respectively, by quadrature integration (i.e., Simpson's rule) to complete the unconstrained-range solution ($\sigma(\phi) = 0$, $\chi(\phi) = \chi_o$ as before).

Neighboring Optimal Control

Assuming that the unconstrained range trajectory can be made to come close to the desired target (ξ_T, η_T, w_T), the process of hitting the target can be accomplished by neighboring optimal control to a perturbed final point. The neighboring optimum formulation is given in Ref. (6), and it is the result of linearizing the first variation conditions about the optimum. The control perturbations vector $\delta\boldsymbol{u}$ to compensate for perturbations in the state vector $\delta\boldsymbol{x}$ and the final conditions $d\Psi_s$ can be stated as

$$\delta u(\phi) = \begin{bmatrix} \delta\lambda \\ \delta\sigma \end{bmatrix} = -H_{uu}^{-1}[(H_{ux} + f_u^T(\bar{S} - \bar{R}\,\bar{Q}^{-1}\bar{R}^T)\delta\boldsymbol{x} + f_u^T\bar{R}\,\bar{Q}^{-1}d\Psi_s] \quad (15)$$

where the following relations exist along the nominal trajectory:

$$\begin{aligned} H_{xx} &= H_{ux} = 0 \\ m &= \Omega_{x_f} = (G_{\phi_f} + H_f)_{x_f} = 0 \\ \bar{S} &= S - mm^T/\alpha = 0 \\ \alpha &= \Omega' = p_w \cos\phi_f/\bar{M} \\ \bar{R} &= R - mn^T/\alpha = R \\ \bar{Q} &= Q - nn^T/\alpha \\ n &= \Psi_f' = f_f \end{aligned} \quad (16)$$

where the notation $(\,)_{\phi_f}$, $(\,)_{x_f}$, $(\,)' = \partial(\,)/\partial\phi_f$, $\partial(\,)/\partial x_f$, $d(\,)/d\phi_f$, respectively, and

$$d\Psi_s = \begin{bmatrix} \xi_T - \xi_{ur} \\ \eta_T - \eta_{ur} \\ 0 \end{bmatrix} \quad (17)$$

subscript f indicates final value. The desired perturbation in the final altitude (or dimensionless density w_f) is zero.

It is desired to compute the optimal control and the neighboring optimal control perturbations at the sample point and hold its value constant over the sample period. Because the state perturbation vector is $\delta\boldsymbol{x} = 0$ at the sample point as the states are updated, the control perturbation vector is given by

$$\delta\boldsymbol{u}_o = -[H_{uu}^{-1}f_u^T R\bar{Q}^{-1}]_{\phi_o}\, d\Psi_s \quad (18)$$

where $d\Psi_s$ and its coefficient are evaluated on the unconstrained-surface-range optimal path. The quantities H_{uu} and f_u are given by

$$H_{uu} = -\begin{bmatrix} \dfrac{2}{\lambda + \bar{M}} & 0 \\ 0 & \dfrac{2}{\lambda + \bar{M}} \end{bmatrix},$$

$$f_u = \begin{bmatrix} \dfrac{\cos\chi_o \cos\phi}{(\lambda + \bar{M})^2 w} & 0 \\ \dfrac{\sin\chi_o \cos\phi}{(\lambda + \bar{M})^2 w} & 0 \\ \dfrac{\sin\phi}{(\lambda + \bar{M})^2} & 0 \\ \dfrac{p_w \sin\phi}{(\lambda + \bar{M})^2} & 0 \\ 0 & -\dfrac{1}{\cos\phi(\lambda + \bar{M})} \end{bmatrix} \quad (19)$$

where $\lambda + \bar{M}$ is given by Eq. (11). R can be calculated by integrating

$$\frac{dR}{d\phi} = -f_x^T R = \begin{bmatrix} 0 & 0 & 0 \\ 0 & 0 & 0 \\ -f_{x_{13}} & -f_{x_{23}} & 0 \\ 0 & 0 & 0 \\ -f_{x_{15}} & -f_{x_{25}} & 0 \end{bmatrix} \quad (20)$$

where

$$f_x = \begin{bmatrix} 0 & 0 & \dfrac{\cos\chi_o \cos\phi}{(\lambda + \bar{M})w^2} & 0 & \dfrac{\sin\chi_o \cos\phi}{(\lambda + \bar{M})w} \\ 0 & 0 & \dfrac{\sin\chi_o \cos\phi}{(\lambda + \bar{M})w^2} & 0 & -\dfrac{\cos\chi_o \cos\phi}{(\lambda + \bar{M})w} \\ 0 & 0 & 0 & 0 & 0 \\ 0 & 0 & 0 & 0 & 0 \\ 0 & 0 & 0 & 0 & 0 \end{bmatrix}$$

$$R_f = \left[\frac{\partial\Psi}{\partial x}\right]^T_{\phi_f} = \begin{bmatrix} 1 & 0 & 0 \\ 0 & 1 & 0 \\ 0 & 0 & 1 \\ 0 & 0 & 0 \\ 0 & 0 & 0 \end{bmatrix}$$

Then, with $R(\phi)$ known, $\bar{Q}$ can be obtained from

$$\frac{dQ}{d\phi} = -R^T f_u^T H_{uu}^{-1} f_u R = -R^T B R, \tag{21}$$

$(Q[\phi_f] = [0])$

$$= \begin{bmatrix} B_{11} + 2R_{31}B_{31} + R_{31}^2 B_{33} + R_{51}^2 B_{55} & & \\ B_{21} + R_{31}B_{32} + R_{32}(B_{31} + R_{31}B_{33}) + R_{51}R_{52}B_{55} & B_{22} + 2R_{32}B_{32} + R_{32}^2 B_{33} + R_{52}^2 B_{55} & \\ B_{31} + B_{33}R_{31} & B_{32} + B_{33}R_{32} & B_{33} \end{bmatrix}$$

where only the lower triangular elements of the symmetric matrix have been shown and individual elements of the R, B matrices are distinguished by numerical subscripts. To prove the feasibility of this method, a Runge-Kutta scheme was used to integrate the R, Q equations; however, a quadrature scheme could be used to gain execution speed given the uncoupled R equation. Note that only four elements of R are needed for the computation of Q. Finally, $\bar{Q}$ is formed as $\bar{Q} = Q - nn^T/\alpha$, where n and α are given in Eq. (16).

Guidance Law

The guidance law or the feedback control law to achieve ξ_T, η_T, and w_T for a given value of $\bar{M}$ is the sum of the optimal control vector,

$$\boldsymbol{u} = \begin{bmatrix} \lambda \\ \sigma \end{bmatrix}$$

in Eqs. (11) and (12) and the neighboring control perturbations, $\delta\boldsymbol{u}$, in Eq. (18), or

$$\boldsymbol{u}_o = \begin{bmatrix} -\sqrt{1 + \bar{M}^2 + p_w \sin\phi_o} - \bar{M} \\ 0 \end{bmatrix} + \begin{bmatrix} -\dfrac{\lambda + \bar{M}}{2} & 0 \\ 0 & -\dfrac{\lambda + \bar{M}}{2} \end{bmatrix} \begin{bmatrix} f_{u_{11}} + f_{u_{31}}R_{31} & f_{u_{21}} + f_{u_{31}}R_{32} & f_{u_{31}} \\ f_{u_{52}}R_{51} & f_{u_{52}}R_{52} & 0 \end{bmatrix} \times \begin{bmatrix} \bar{Q}_{11}^{-1}(\xi_T - \xi_{ur}) + \bar{Q}_{21}^{-1}(\eta_T - \eta_{ur}) \\ \bar{Q}_{21}^{-1}(\xi_T - \xi_{ur}) + \bar{Q}_{22}^{-1}(\eta_T - \eta_{ur}) \\ \bar{Q}_{31}^{-1}(\xi_T - \xi_{ur}) + \bar{Q}_{32}^{-1}(\eta_T - \eta_{ur}) \end{bmatrix} \tag{22}$$

where individual elements of f_u, R, and $\bar{Q}^{-1}$ are distinguished by numerical subscripts. At each sample point, the value of $\bar{M}$ is updated from inertial measurements. To summarize the guidance calculations in algorithmic form we should compute the following for each sample point update:

1) the nominal quantities:

a) ϕ_o, $\bar{M}$, w_o from the sample point update values of γ_o, $\rho_o(h_o)$, V_o using Eq. (7);

b) p_w from Newton iteration on Eq. (14) by integrating from the sample point ϕ_o to a guessed ϕ_f, using Eq. (11) for $\lambda + \bar{M}$ and Eq. (13) for the guessed value of $\phi_f(p_w)$, [where $w(\phi_f) = w_T$, and $w_T(\rho_T(h_T = 0))$ from Eq. (7) needs to be computed once for an entire flight]; and

c) ξ_{ur}, η_{ur} by integrating Eqs. (2) and (3) from the sample point ϕ_o (and χ_o) to the now known value of ϕ_f.

2) the neighboring optimal quantities (evaluated about the nominal planar trajectory)

a) $d\Psi_s$ from Eq. (17) [the target values, ξ_T, η_T need to be computed only once per flight from Eq. (7)];

b) $H_{uu}(\phi_o)$, $f_u(\phi_o)$ from Eq. (19) using the sample point values, ϕ_o, χ_o,

c) $R(\phi_o)$ by integrating Eq. (20) backward from the nominal computed ϕ_f to the sample point ϕ_o;

d) $Q(\phi_o)$ by integrating Eq. (21) backward from the nominal computed ϕ_f to the sample point ϕ_o; and

e) $\boldsymbol{u}_o$ from Eq. (22) by adding the nominal components, evaluated at the sample point using Eq. (11) and $\sigma(\chi_o) = 0$, to the neighboring optimal perturbations.

Again, these computed controls will be held constant for the sample period.

To demonstrate the effectiveness of this guidance law, it has been flown in a three-DOF (point-mass) simulation containing a "true" time-based physical flight model, a standard atmosphere, and wind-tunnel-based aerodynamics. Results are shown in Figs. 2–5 for a sample period of $\Delta t = 0.1$ s.

Also shown in these figures are the open-loop optimal (i.e., parameter optimization) trajectory for the simulation model and the trajectory obtained from proportional navigation (PRONAV). The open-loop optimal trajectory has been obtained for a piecewise-linear control (suboptimal control) using recursive quadratic programming (RQP).[9] The PRONAV guidance law is that of the linear-quadratic control law of Ref. 10. Weighting is for miss distance only, leading to the familiar control gain $K = 3/t_{go}^2$, where t_{go} is calculated at each sample point as range-to-go/range-rate.

A fourth-order, fixed step, Runge-Kutta integrator is used in all simulations. The trajectory boundary conditions for the example problem are shown in Table 1.

Fig. 2 displays the simulation flight path profiles. The neighboring optimal guidance and RQP have the same general "glide-and-dive" contour, vs PRONAV, which turns quickly to line up with the target. As first seen in Ref. 3, these first two simulations shift the majority of flight time to the higher altitudes, where drag is low.

Velocity–time profiles in Fig. 3 are grouped in a similar fashion to the flight profiles. Because of the altitude management in the proposed guidance and the RQP guidance, the terminal velocities show small differences. The true optimal velocity produced by the RQP scheme is 6497 ft/s. The terminal velocity generated by the proposed method differs from it by about 1%, while the PRONAV solution is over 40% less. Note

Table 1 Trajectory boundary conditions

	Initial	Final
downrange, nm	0	70
crossrange, nm	0	15
altitude, ft	100,000	0
velocity, ft/s	11,000	maximum
γ, deg	0	unconstrained
χ, deg	0	unconstrained

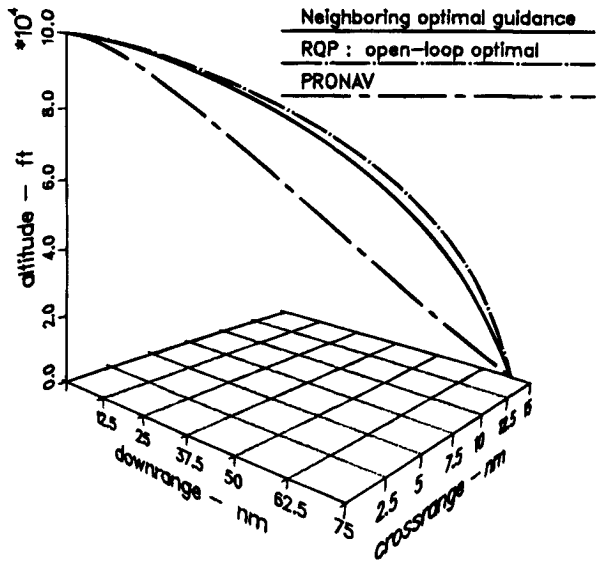

Fig. 2 Flight path comparisons.

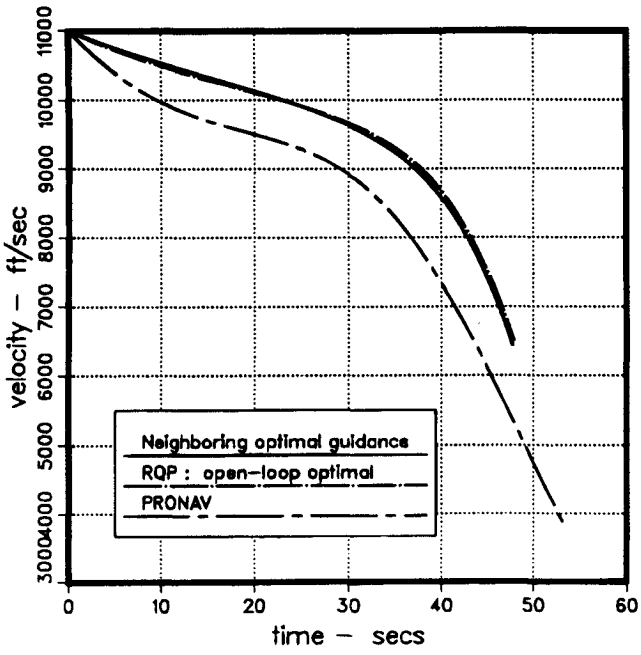

Fig. 3 Velocity comparisons.

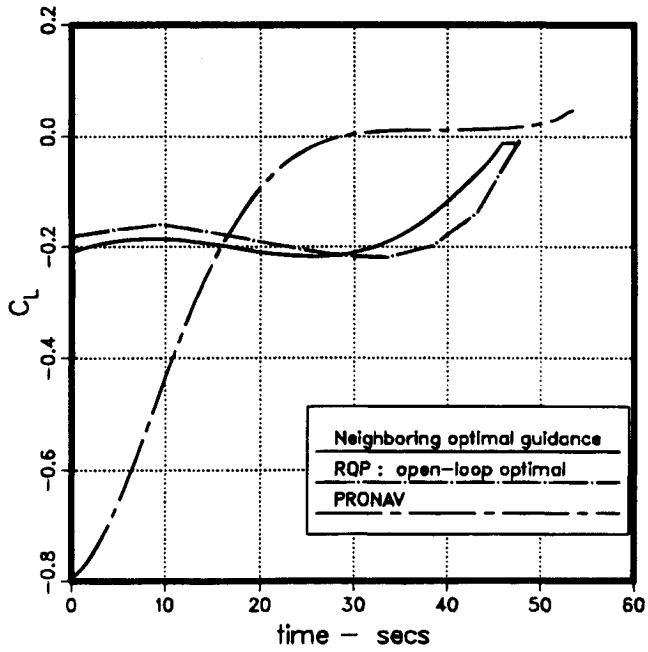

Fig. 4 Lift coefficient comparisons.

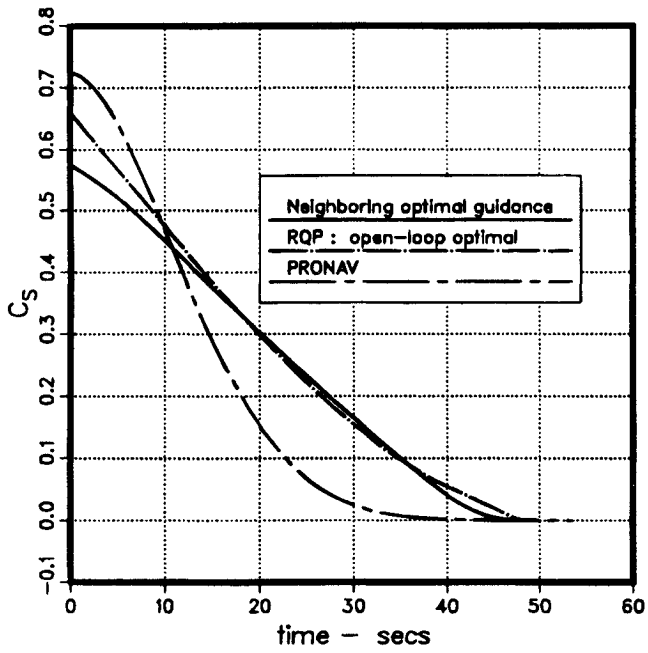

Fig. 5 Side-force coefficient comparisons.

also that the times of flight for these two simulations are almost identical.

The lift coefficient, $C_L = C_L^*\lambda$, profiles shown in Fig. 4 reconfirm the turning rates between PRONAV and the other guidance schemes. The "corners" in the RQP simulation are the *node* points at which the parameter controls are obtained. The open-loop optimal scheme seems to take advantage of the increased dynamic pressure near the end of the trajectory to apply increased negative lift. Note that the natural boundary condition $C_{L_f}(=\lambda_f) = 0$ is approximately satisfied for the neighboring optimal and exactly satisfied for RQP. (Both lift and side-force values were frozen in the proposed guidance scheme, when the current velocity vector penetrated the ground within a 50-ft radius circle of the target, to prevent large gain computations as the range-to-target approached zero).

The side-force coefficient, $C_S = C_L^*\sigma$, profiles are shown in Fig. 5 and also show the increased turning rate applied by PRONAV to line up with the target. The open-loop optimum initially chooses a middle ground between PRONAV and the proposed scheme. Note that all of these schemes approach a final value, $\sigma_f = 0$, indicating that the velocity vector is aligned with the target at impact.

To demonstrate the targeting flexibility insofar as deliverable terminal velocity, the propose scheme was compared against PRONAV for several turn geometries. The demands presented by these choices range from a fairly short, tight turn to a lofting, gradual turn. The terminal velocities, ft/s, are shown in Table 2.

Table 2 Terminal velocities

	Proposed	PRONAV
Crossrange, nm	20	20
Downrange, nm		
40	4146	873
80	6232	2666
120	6415	830

The initial unconstrained range was 71.5 nm. For this particular crossrange, the proposed method delivers consistently high terminal velocities for a considerable change in downrange, whereas the PRONAV solution has a narrow band of effectiveness.

As a midcourse guidance proposal, this scheme is capable of flying to the target with acceptable position-error residuals, but it is recommended to switch to a terminal scheme for more precise target acquisition.

Conclusions

A sampled-data feedback control method has been devised to obtain approximate, maximum-terminal-velocity descent trajectories at a designated target. These trajectories are characterized by glide-and-dive flight to the target to minimize the time spent in the denser parts of the atmosphere. The proposed online scheme uses neighboring optimal theory to successfully bring final altitude and range constraints together, as well as to compensate for differences in flight model, atmosphere, and aerodynamics. Comparison with the open-loop optimal trajectory for the terminal velocity is excellent and far exceeds the proportional navigation solution for a variety of targeting geometries.

Acknowledgment

This work was performed at Sandia National Laboratories and was supported by the U.S. Department of Energy under contract DE-AC04-76DP00789.

References

[1] Contensou, P., "Contribution à' l'Etude Schematique des Trajectories Semi-Balistique à' Grand Portée," Communication to Association Technique Maritime et Aeronautique, Paris, 1965.

[2] Busemann, A., Vinh, N. X., and Kelley, G. F., "Optimum Maneuvers of a Skip Vehicle with Bounded Lift Constraints," *JOTA*, Vol. 3, 1969, pp. 243–262.

[3] Eisler, G. R., and Hull, D. G., "Guidance Law for Planar Hypersonic Descent to a Point," *Journal of Guidance, Control, and Dynamics*, Vol. 16, No. 2, 1993, pp. 400–402.

[4] Bryson, A. E., and Ho., Y. C., *Applied Optimal Control*, Halsted Press, New York, 1975.

[5] Speyer, J. L., and Bryson, A. E., "A Neighboring Optimum Feedback Control Scheme Based on Estimated Time-to-Go with Applications to Re-Entry Flight Paths, *AIAA Journal*, Vol. 6, No. 5, 1968.

[6] Kumar, R. R., Seywald, H., and Cliff, E. M., "Near Optimal 3-D Guidance Against a Maneuvering Target," *1989 AIAA Guidance, Navigation, and Control Conference* (Boston, MA), AIAA, Washington, DC, 1989, pp. 482–495.

[7] Loh, W. H. T., *Dynamics and Thermodynamics of Planetary Entry*, Prentice-Hall, Englewood Cliffs, NJ, 1963.

[8] Eisler, G. R., "Maximum-Terminal-Velocity Guidance for a Hypersonic Glider", Ph.D Dissertation, Univ. of Texas at Austin, Austin, TX, May 1986.

[9] Powell, M. J. D., "A Fast Algorithm for Nonlinearly Constrained Optimization Calculations", *Proceedings of the Biennial Conference on Numerical Analysis, 28 June–1 July 1977*, Springer-Verlag, Berlin, 1978, pp. 144–157.

[10] Riggs, T. L., and Vergez, P. L., "Advanced Air-to-Air Missile Guidance Using Optimal Control and Estimation," Air Force Armament Laboratory, AFATL-TR-81-56, June 1981.